Journal of Contaminant Hydrology 159 (2014) 57–66

Contents lists available at ScienceDirect

Journal of Contaminant Hydrology

journal homepage: www.elsevier.com/locate/jconhyd

Estimation and upscaling of dual-permeability model parameters for the transport of *E. coli* D21g in soils with preferential flow

Yusong Wang [a,*], Scott A. Bradford [b], Jiří Šimůnek [a]

[a] Department of Environmental Sciences, University of California, Riverside, CA 92521, United States
[b] USDA, ARS, Salinity Laboratory, Riverside, CA, United States

ARTICLE INFO

Article history:
Received 13 October 2013
Received in revised form 25 January 2014
Accepted 31 January 2014
Available online 7 February 2014

Keywords:
Microorganism
Transport
Preferential flow
Dual-permeability model

ABSTRACT

Dual-permeability models are increasingly used to quantify the transport of solutes and microorganisms in soils with preferential flow. An ability to accurately determine the model parameters and their variation with preferential pathway characteristics is crucial for predicting the transport of microorganisms in the field. The dual-permeability model with optimized parameters was able to accurately describe the transport of *E. coli* D21g in columns with artificial macropores of different configurations and lengths at two ionic strength levels (1 and 20 mM NaCl). Correlations between the model parameters and the structural geometry of the preferential flow path were subsequently investigated. Decreasing the macropore length produced a decrease in the apparent saturated hydraulic conductivity of the macropore domain and an increase in the mass transfer between the macropore and matrix domains. The mass transfer coefficient was also found to be dependent on the configuration of the preferential flow pathway. A linear superposition approach was used to estimate field-scale preferential transport behavior for hypothetical fields with different amounts and configurations of macropores. Upscaling procedures were numerically investigated to predict this field-scale transport behavior from column-scale parameters. The upscaling method provided a satisfactory prediction of the field results under the tested scenarios. This information will be useful in assessing the risks of microbial transport due to preferential flow.

1. Introduction

Surface and groundwater contamination by pathogenic microorganisms has been reported across the United States, which put the public's health at risk (Abbaszadegan et al., 2003; Borchardt et al., 2003; USEPA, 1997). Water entering groundwater has to pass through porous media in the vadose and saturated zones in the subsurface. Soil passage, such as riverbank filtration, dune recharge, infiltration basins and trenches, and sand filters, is also used to treat surface water to meet demands for drinking water (Schijven and Hassanizadeh, 2000). Therefore, an accurate understanding of the transport and fate of pathogens in porous media is needed to protect our drinking water resources.

Many studies have been conducted to quantify the influence of physical (size of the microbe and the porous medium, microbe concentration, water velocity, water content and surface roughness) and chemical (surface chemistry of the microbe and soil, and aqueous solution pH, ionic strength, and chemical composition) factors on microorganism transport in homogeneous porous media (Bradford et al., 2006; Chen and Walker, 2007; Dong et al., 2002; Hendry et al., 1999; Mccaulou et al., 1995; Mills et al., 1994; Yee et al., 2000). However, field experiments have frequently revealed that preferential pathways are a major contributor to the overall transport of microbes because they are typically strongly retained in the soil matrix (Abu-Ashour et al., 1994; Bales et al., 1989; Jiang et al., 2010).

* Corresponding author. Tel.: +1 951 823 9431.
E-mail address: Ywang032@ucr.edu (Y. Wang).

0169-7722/$ – see front matter © 2014 Elsevier B.V. All rights reserved.
http://dx.doi.org/10.1016/j.jconhyd.2014.01.009

The occurrence of preferential flow is found to be the rule rather than the exception in most field soils (Flury et al., 1994; Singh and Kanwar, 1991), which may occur as a result of plant roots, burrowing earthworms, cracks, or natural structural heterogeneities (Beven and Germann, 1982; Cey et al., 2009; Madsen and Alexander, 1982; Unc and Goss, 2003; Wollum and Cassel, 1978). Preferential flow has been identified as a major problem hampering accurate predictions of contaminant transport in soils because of difficulty in quantifying the physical and chemical complexities of the soil matrix and macropore system (Šimůnek et al., 2003).

The study of preferential flow and transport through artificial macropores provides an opportunity to overcome many modeling challenges in natural soils because the macropore geometry and hydraulic properties can be well defined and controlled in a repeatable manner (Arora et al., 2011, 2012; Castiglione et al., 2003; Guzman et al., 2009; Pivetz and Steenhuis, 1995). Artificial macropores can be systematically created by leaving small cylindrical openings in repacked columns (Castiglione et al., 2003; Pivetz and Steenhuis, 1995) or by packing different sized sands to generate layers and/or lens with contrasting hydraulic conductivities (Bradford et al., 2004; Fontes et al., 1991; Morley et al., 1998; Saiers et al., 1994; Wang et al., 2013, 2014). Controlled preferential flow and transport studies make it possible to isolate and identify factors that have the greatest influence on preferential flow and transport, and provide valuable information on parameterization that is needed to help adapt numerical models to complex natural systems.

Several approaches have been developed to simulate preferential flow and transport (Köhne et al., 2009a,b). One method is to construct a 2D/3D simulation profile by explicitly defining the heterogeneities or the preferential pathways of the domain (e.g., Schelle et al., 2013). Wang et al. (2013, 2014) successfully applied Hydrus 2D/3D to simulate microorganism transport in columns with artificial macropores. A map of the structural geometry must be known in order to conduct the simulation. Some lab-scale mapping methods have been developed to accurately measure pore sizes and connectivity of macropore-type preferential pathways (Anderson et al., 2003; Monga et al., 2007), but this is extremely difficult, if not impossible, in the field.

Other physically based models, such as dual-porosity and dual-permeability models, mostly divide the soil into two or multiple domains, and assume uniform flow within each flow domain. Both dual-porosity and dual-permeability models assume that the porous medium consists of two interacting regions, one associated with the inter-aggregate, macropore, or fracture system, and one comprising intra-aggregate pores inside soil aggregates. While dual-porosity models assume that water in the matrix is stagnant, dual-permeability models allow for water flow in the matrix as well. The mass exchange between the two regions normally is assumed to be linear (Leij and Bradford, 2009). Dual-permeability models are increasingly used for analysis of preferential transport both on the laboratory column-scale (e.g., Allaire et al., 2002; Allaire-Leung et al., 2000; Castiglione et al., 2003; Greco, 2002; Gwo et al., 1995, 1996) and on the plot- or field-scale (e.g., Andreu et al., 1994; Jarvis et al., 1991; Kohler et al., 2001; Larsson and Jarvis, 1999a,b). However, the difficulty in determination of the many dual-permeability model parameters largely limits the application of these models (Köhne et al., 2009a,b).

Stochastic models have also been employed to simulate preferential flow and transport in soils. A variety of stochastic methods have been used to describe solute transport in heterogeneous flow fields (e.g., Dagan, 1984; Freyberg, 1986; Gelhar and Axness, 1983; Kabala and Sposito, 1991; Russo, 1991; Sposito and Barry, 1987). In a simplified stochastic modeling approach the field may be viewed as a series of independent stream tubes with their hydraulic conductivity and/or other selected parameters described using probability density functions (PDFs) (Dagan, 1993; Jury and Roth, 1990). However, no methodology has been developed to directly characterize the PDF, especially when preferential flow pathways are presented. Kung et al. (2005) proposed an indirect method to determine pore-size spectrum of macropore-type preferential pathways, but quantification of PDFs remains a challenge for the application of stochastic models to preferential flow and transport.

The objectives of this study were to link the parameters of the dual-permeability model with geometry information of the macropore, and then investigate methods to upscale behavior from the column- to field-scales. In particular, the dual-permeability model was employed to simulate bromide and microorganism transport in columns with preferential pathways of different lengths and configurations. Correlations were then established between macropore geometry information (length, configuration) and parameters of the dual-permeability model. A linear superposition approach was used to estimate field-scale preferential transport behavior for hypothetical PDFs. Upscaling procedures were numerically investigated to predict the field-scale transport behavior.

2. Experiment information

Transport experiments for *E. coli* D21g were conducted in columns with artificial preferential flow pathways as described by Wang et al. (2013, 2014). Detail information about the column experiments can be found in these publications, and will be briefly summarized below. Two types of Ottawa (quartz) sand with the median grain size of 120 and 710 μm (referred to as fine sand and coarse sand below) were used in the column experiments after being cleaned using a salt cleaning method (Bradford and Kim, 2010) to eliminate any background interference from clay particles. A 13.2 cm diameter by 22 cm long plexiglass column with an 18 μm nominal pore size polyester membrane at the bottom was used in the experiment. The fine sand was wet packed in the column with a plastic tube (with outside diameter of 1.14 cm) in the center. Then the coarse sand and fine sand were filled into the hole created by pulling out the plastic tube from the column to make the desired preferential flow path as described in Fig. 1. Various NaCl and NaBr solutions at selected ionic strength (IS = 1 and 20 mM) with pH = 5.8 were prepared for the experiment. These IS levels were selected to create a range of adhesive conditions between the microorganisms and sand.

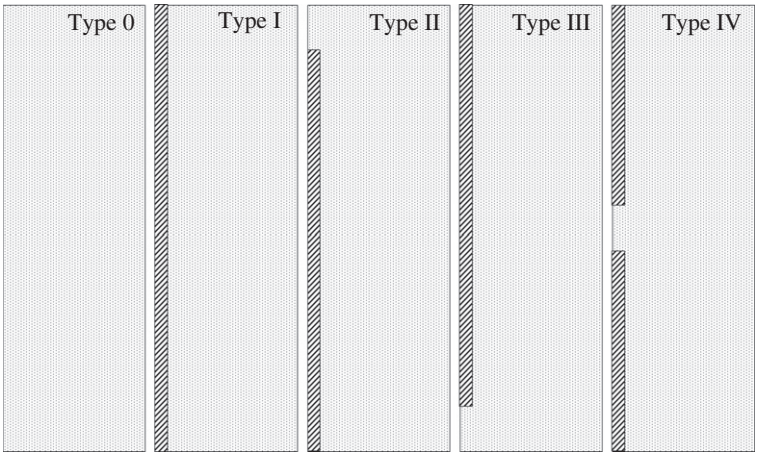

Fig. 1. Axi-symmetric representation of the five types of lens structures (column center is on the left hand side) studied in this research: Type 0—homogeneous fine sand column with no lens, Type I—one lens through the whole column, Type II—one lens opened to the bottom boundary, Type III—one lens opened to the top boundary, and Type IV—a discontinuous lens opened to both boundaries (diagonal pattern represents coarse sand and point pattern represents fine sand).

Solutions were delivered onto the top of the column at a steady flow rate using a rain simulator, and the bottom boundary pressure was maintained at 0 cm by a hanging water column. The column was kept saturated during the experiment by maintaining a shallow depth (<5 mm) of ponding at the surface boundary. The sand in the column was equilibrated by flushing the column with two pore volumes (PVs) of a selected NaCl solution (phase 0) before initiating a microbial transport experiment. Then, several PVs of NaBr solution containing *E. coli* D21g at a concentration of ~1.0×10^8 cells/mL were introduced into the column at a constant rate and IS (phase I), followed by NaCl solution at the same flow rate and IS as in phase I until the effluent microbe concentration returned to a baseline level (phase II). Effluent samples were continuously collected during the transport experiment at selected intervals using a fraction collector, and then analyzed for Br and microbe concentrations.

3. Numerical modeling

Dual-permeability models describe preferential flow using one equation for flow in the matrix and one for flow in the macropore system, with the two flow regions coupled by a water transfer term:

$$\frac{\partial \theta_f}{\partial t} = \frac{\partial}{\partial z}\left(K_f \frac{\partial h_f}{\partial z} - K_f\right) - \frac{\Gamma_w}{w_f} \tag{1a}$$

$$\frac{\partial \theta_m}{\partial t} = \frac{\partial}{\partial z}\left(K_m \frac{\partial h_m}{\partial z} - K_m\right) - \frac{\Gamma_w}{1-w_f} \tag{1b}$$

where the subscript "*m*" represents the matrix, the subscript "*f*" defines a property of the faster macropore system, θ [−] is the water content, h is the pressure head [L, L denotes the units of length], K denotes the saturated hydraulic conductivity [LT^{-1}, T denotes the units of time], w_f is the fraction of total soil occupied by the macropore system ($0 < w_f < 1$), and Γ_w is the water transfer term (T^{-1}). Γ_w is assumed to be proportional to the pressure head difference between the macropore and matrix system, h_f–h_m. Thus, Γ_w equals 0 under saturated, steady-state flow conditions.

Modified convection–dispersion equations were used to describe transport and deposition of microorganisms in both the macropore and matrix regions:

$$\frac{\partial\left(\theta_f C_f\right)}{\partial t} = -\frac{\partial J_f}{\partial z} - E_f - \frac{\Gamma_s}{w_f} \tag{2a}$$

$$\frac{\partial(\theta_m C_m)}{\partial t} = -\frac{\partial J_m}{\partial z} - E_m - \frac{\Gamma_s}{1-w_f} \tag{2b}$$

where C [$N_c L^{-3}$; N_c denotes the number of microbes] is the microbe concentration in the aqueous phase, J [$N_c L^{-2}\ T^{-1}$] is the microbe flux (sum of the advective and dispersive fluxes), the mass transfer rate between the macropore and matrix regions Γ_s is given as

$$\Gamma_s = k_{fm}\left(1-w_f\right)\theta_m\left(C_f - C_m\right) + \Gamma_w C^{\#} \tag{3}$$

where k_{fm} is a first-order diffusive mass transfer coefficient (T^{-1}), $C^{\#}$ is equal to C_m for $\Gamma_w > 0$ and C_f for $\Gamma_w < 0$, and E is the mass transfer function from the aqueous phase to/from the solid–water interface as:

$$E = \frac{\partial(\rho S)}{\partial t} = \theta\psi k_{att} C - \rho k_{\mathrm{det}} S \tag{4}$$

where S [$N_c M^{-1}$; M denotes units of mass of soil] is the microbe concentration on the solid phase, k_{det} [T^{-1}] is the microbe detachment rate coefficient, k_{att} [T^{-1}] is the microbe attachment rate coefficient, and ρ [ML^{-3}] is the bulk density. The parameter ψ [-] accounts for time and concentration dependent blocking using a Langmuirian approach as (Adamczyk et al., 1994):

$$\psi = 1 - \frac{S}{S_{\max}} \tag{5}$$

where S_{max} [N_c M^{-1}] is the maximum solid phase concentration of microbes.

The simulations were carried out with the HYDRUS-1D code (Šimůnek et al., 2008). A constant positive pressure head was applied at the column inlet as a shallow depth of ponding was maintained at the surface of the column, and a constant zero pressure head was employed at the outlet for the water flow boundary. A third-type boundary condition was employed at the column inlet and a zero concentration gradient was used at the outlet for these simulations. Some of the model parameters were determined experimentally or using a nonlinear least squares optimization routine in HYDRUS-1D by the same method as described in our previous studies (Wang et al., 2013, 2014). In brief, K_m, θ_m, θ_f, and w_f were directly measured, and retention parameters (k_{att}, k_{det}, and S_{max}) were optimized in HYDRUS-1D with data from homogeneous column experiments. Some other parameters (e.g., K_f and k_{fm}) were also determined using a nonlinear least squares optimization routine in HYDRUS-1D.

4. Results and discussion

Results from the transport experiments for *E. coli* D21g in columns with preferential flow paths of different lengths and configurations (Wang et al., 2013, 2014) were used to investigate the relationship between the geometry properties of the preferential path and parameters of the dual-permeability model. Breakthrough data of bromide was first used to characterize parameters for water flow before looking into the transport of *E. coli* D21g.

4.1. Transport of bromide

The transport of bromide depended on the following parameters during saturated, steady-state flow conditions: saturated hydraulic conductivities of the matrix (K_m) and the macropore (K_f), saturated water content of the matrix (θ_m) and the macropore (θ_f), dispersivities of the matrix (λ_m) and the macropore (λ_f), the ratio of the volumes of the macropore domain and the total column system (w_f), and the mass transfer rate at the interface between matrix and macropores (k_{fm}). The saturated hydraulic conductivity of the matrix, K_m, was considered as a constant for all cases based on the value in the homogeneous column. However, due to variation caused by packing, K_m was determined by the arrival time of the bromide pulse from the matrix for each column experiment (Wang et al., 2013). We set the dispersivities of the matrix and the macropore to the values obtained from homogeneous column experiments of fine sand and coarse sand, respectively (Wang et al., 2013). The porosities of both matrix and macropore were set to the measured values in homogeneous column experiments. The parameter w_f was calculated based on the volume of the macropore and the total column with Type I lens configuration (cf. Fig. 1), and the same value was used for other lenses with different lengths and configurations. The values of these parameters are listed in Table 1.

Since K_m and w_f were set as constants, K_f was the main parameter which determined the relative concentration of bromide in the first pulse that was associated with preferential transport. When the length of the lens decreased, the relative contribution of preferential transport decreased and arrival time of the preferential transport was delayed. Consequently, K_f decreased with a decrease in the length of the lens for all three types of lens configurations (Table 1). For the same lens length, the value of K_f for the Type IV lens configuration was smaller than that of Type II and Type III. This was consistent with the observation that the Type IV lens configuration had a later arrival and a smaller amount of preferential transport compared to Type II and Type III lens configurations.

Larger dispersion was reported for Type IV lens configuration compared to Type II and Type III configurations (Wang et al., 2014), which indicated greater mixing at the interface between the matrix and the macropore domains. The greater mixing at the interface for Type IV lens configuration was reflected by the larger mass transfer coefficient in the dual-permeability model as shown in Table 1. The mass transfer coefficient for Type IV configuration was almost independent of the length of the lens. However, the mass transfer coefficient increased with a decrease in the length for Type II and Type III lens configurations. Fig. 2 shows selected examples of observed BTCs for bromide and corresponding simulations with parameters in Table 1.

Table 1 indicates that the macropore geometry had a great effect on both the hydraulic conductivity of the macropore (K_f) and the mass transfer coefficient between the macropore and matrix (k_{fm}). Recall that the experimental macropore consisted of a specific length and location of coarse textured sand lenses that were embedded in the center of the matrix sand. Conversely, the simulated macropore geometry in the dual permeability model was the same for all configurations, and was equal to the column length. Consequently, the hydraulic properties of the simulated macropore changed

Table 1
Model parameters obtained from previous studies and optimized saturated conductivities of the fracture, K_f, and mass transfer coefficients for bromide, k_{fm}, and their 95% confidence intervals.

Lens configuration	Lens length (cm)	K_m (cm/min)	θ_m	θ_f	λ_m (cm)	λ_f (cm)	w_f	K_f (cm/min)	k_{fm} (min^{-1})
Type I	20	0.31	0.36	0.36	0.10	0.55	0.00746	10.9 ± 0.5	(1.40 ± 0.7) * 10^{-4}
Type II	19	0.32	0.36	0.36	0.10	0.55	0.00746	8.3 ± 0.7	(1.37 ± 1.2) * 10^{-4}
Type II	18	0.30	0.36	0.36	0.10	0.55	0.00746	7.8 ± 0.7	(2.35 ± 1.0) * 10^{-4}
Type II	16	0.32	0.36	0.36	0.10	0.55	0.00746	6.2 ± 0.7	(2.82 ± 1.5) * 10^{-4}
Type II	10	0.34	0.36	0.36	0.10	0.55	0.00746	4.0 ± 0.7	(5.91 ± 3.1) * 10^{-4}
Type III	19	0.32	0.36	0.36	0.10	0.55	0.00746	9.7 ± 0.9	(1.60 ± 1.0) * 10^{-4}
Type III	16	0.32	0.36	0.36	0.10	0.55	0.00746	6.7 ± 1.1	(2.86 ± 2.0) * 10^{-4}
Type IV	19	0.32	0.36	0.36	0.10	0.55	0.00746	8.1 ± 0.8	(5.80 ± 1.7) * 10^{-4}
Type IV	18	0.32	0.36	0.36	0.10	0.55	0.00746	7.1 ± 0.8	(5.40 ± 2.1) * 10^{-4}
Type IV	16	0.32	0.36	0.36	0.10	0.55	0.00746	4.2 ± 0.7	(5.27 ± 2.3) * 10^{-4}

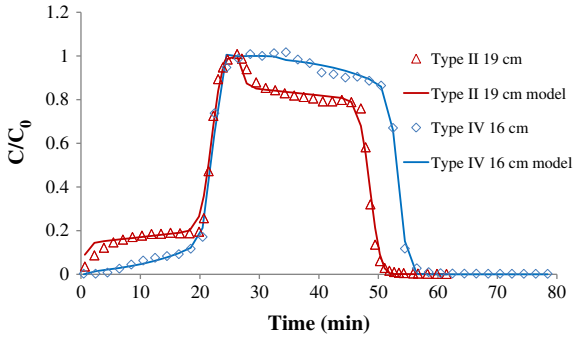

Fig. 2. Observed and simulated BTCs of bromide from columns of Type II 19 cm and Type IV 16 cm.

with the experimental length and location of the macropore. In particular, the value of K_f decreased with decreasing length of the experimental macropore because greater amounts of the flow occurred in the matrix material which had a smaller hydraulic conductivity. A decrease in lens length also produced a corresponding increase in k_{fm}. For the same lens length, the Type IV lens configuration tended to produced higher values of k_{fm} than the Type II and III lenses, because of differences in the number of interruptions (lens–matrix interfaces) to the preferential flow path (cf., Fig. 1). Each interruption tended to slow down water flow and transport, and enhance the exchange process. This explains why the Type IV lens configuration was associated with smaller K_f and larger k_{fm}, than Type II and III lenses.

4.2. Transport of E. coli D21g

After obtaining the information required to describe water flow and transport of the conservative tracer, the transport of *E. coli* D21g should be well quantified with the retention parameters of *E. coli* D21g (microbe attachment rate coefficient, k_{att}; microbe detachment rate coefficient, k_{det}; maximum solid phase concentration of microbes, S_{max}) obtained from homogeneous experiments under the same conditions by Wang et al. (2013) (Table 2). However, forward simulations based on these parameters had relatively poor agreement with most of the experimental results.

At low IS (1 mM), when there was little retention of *E. coli* D21g in both the matrix and lens, forward simulations had a later arrival time for transport in the matrix and a lower concentration for transport in the preferential path. This phenomenon was attributed to size exclusion by Wang et al. (2014). The saturated water content of the macropore (θ_f) and matrix (θ_m) were therefore optimized to account for the influence of size exclusion on the transport data of *E. coli* D21g at low IS. The mass transfer coefficient k_{fm} was also optimized, and the retention parameters were obtained from homogeneous experiments. A summary of model parameters is given in Table 2. Smaller θ_m and θ_f were obtained from *E. coli* D21g compared to bromide. This observation is consistent with the assumption that size exclusion increased the transport velocity of *E. coli* D21g by constraining cells to faster flow domains and larger pore networks than bromide (Wang et al., 2014). The mass transfer coefficients of *E. coli* D21g at low IS were quite close to that of bromide for the same lens configuration. Fig. 3 shows an example of observed BTCs for *E. coli* D21g at IS = 1 mM and simulations with parameters in Tables 1 and 2.

At high IS (20 mM), forward simulations tended to have higher concentrations for the breakthrough from the preferential path. Table 2 presents the mass transfer coefficient k_{fm} that was optimized to better describe the transport of *E. coli* D21g at high IS, and the retention parameters that were obtained from the homogeneous experiments. The mass transfer coefficients for *E. coli* D21g at high IS were significantly greater than that for bromide for the same lens configuration and length. Similar to the trend with bromide, the mass transfer coefficient increased with a decrease in the lens length, and the Type IV lens configuration had a greater transfer rate than Type II and Type III lens configurations of the same length. Examples of observed BTCs for *E. coli* D21g at IS = 20 mM and simulations with parameters in Tables 1 and 2 are given in Fig. 4.

5. Upscaling approach

5.1. Virtual field

In order to investigate the ability of the dual-permeability model to simulate the transport of *E. coli* D21g at larger scales, we generated virtual fields with a distribution of preferential

Table 2
Retention parameters for the matrix used in simulations (k_{det} for the matrix and k_{att}, S_{max}, and k_{det} for the macropore were set as 0 as they were extremely small), and optimized saturated water content of the fracture (θ_f) and matrix (θ_m), the ratio of saturated conductivities optimized from *E. coli* D21g to that optimized from bromide for the fracture and matrix (θ_m/θ^*_m and θ_f/θ^*_f, respectively), and mass transfer coefficients, k_{fm}, for *E. coli* D21g at 1 and 20 mM, and their 95% confidence intervals.

Lens configuration	Lens length (cm)	IS (mM)	k_{att}	S_{max}	θ_m	θ_m/θ^*_m	θ_f	θ_f/θ^*_f	k_{fm} (min^{-1})
Type II	19	1	0.0004	0.01	0.327 ± 0.002	0.91	0.313 ± 0.03	0.87	$(1.97 \pm 1.2) * 10^{-4}$
Type III	19	1	0.0004	0.01	.333 ± 0.003	0.93	0.265 ± 0.02	0.74	$(2.98 \pm 1.1) * 10^{-4}$
Type IV	19	1	0.0004	0.01	.339 ± 0.003	0.94	0.263 ± 0.02	0.73	$(5.80 \pm 1.6) * 10^{-4}$
Type I	20	20	0.2	3.5	NA[a]	NA[a]	NA[a]	NA[a]	$(4.40 \pm 0.38) * 10^{-4}$
Type II	19	20	0.2	3.5	NA[a]	NA[a]	NA[a]	NA[a]	$(5.27 \pm 0.62) * 10^{-4}$
Type II	18	20	0.2	3.5	NA[a]	NA[a]	NA[a]	NA[a]	$(1.28 \pm 0.15) * 10^{-3}$
Type II	16	20	0.2	3.5	NA[a]	NA[a]	NA[a]	NA[a]	$(2.31 \pm 0.89) * 10^{-3}$
Type IV	19	20	0.2	3.5	NA[a]	NA[a]	NA[a]	NA[a]	$(6.39 \pm 0.58) * 10^{-4}$
Type IV	18	20	0.2	3.5	NA[a]	NA[a]	NA[a]	NA[a]	$(2.96 \pm 0.61) * 10^{-3}$
Type IV	16	20	0.2	3.5	NA[a]	NA[a]	NA[a]	NA[a]	NA[a]

[a] Not available due to the low concentration in collected effluent.

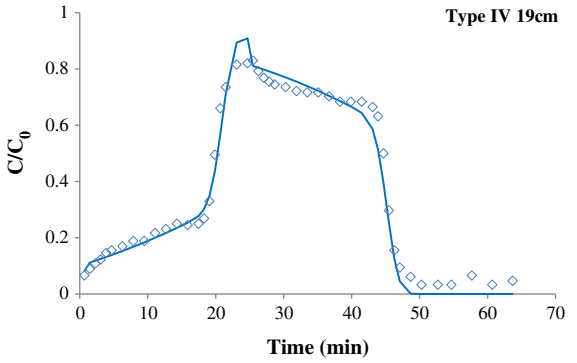

Fig. 3. Observed and simulated BTCs of *E. coli* D21g at IS = 1 mM from column of Type IV 19 cm.

pathways. The virtual fields consisted of independent "stream tubes" that were run in parallel (e.g., no interaction between the stream tubes). Transport within each individual stream tube was consistent with the results of a particular column experiment with selected macropore length and configuration, and solution ionic strength (Figs. 3 and 4; Table 2). The virtual field was comprised of selected fractions of each column type. Table 3 shows some examples of virtual fields with their fractions, f_i, of each column unit. The fractions of all column units were randomly allocated with the same probability to cover a wide range of possible situations.

The stream tube model does not consider lateral exchange between stream tubes. This assumption is justified in our virtual fields because all of the stream tubes have the same matrix properties and simulations demonstrate that the water flow at

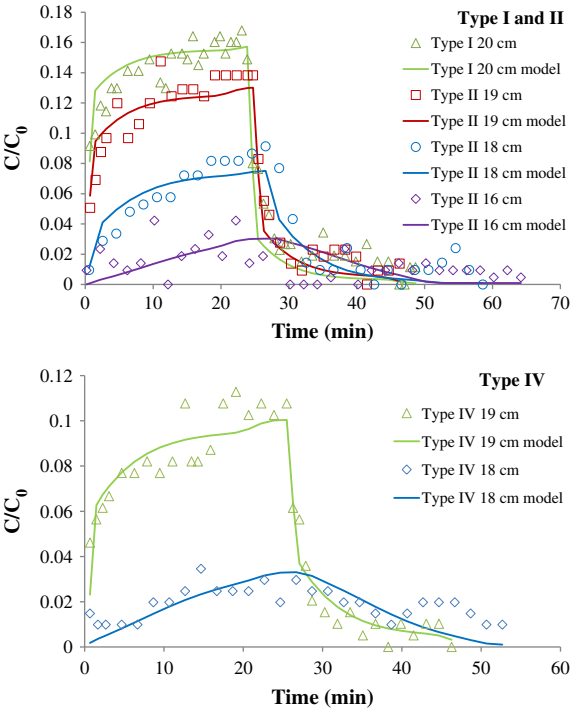

Fig. 4. Observed and simulated BTCs of *E. coli* D21g at IS = 20 mM.

the outside boundary of the stream tube is essentially 1D in the vertical direction (Wang et al., 2013). In this work, we use the dual-permeability model to account for flow and transport within a given stream tube (column). The dual-permeability model considers lateral exchange between the matrix and macropore and two advective fluxes within a given stream tube (column); see Eqs. (1a)–(3). Consequently, the inclusion of the dual-permeability model into the stream tube method is an advantage because it provides one way to account for lateral exchange, as well as variations in advection.

Simulations were carried out for each column unit with IS equaled to 1 and 20 mM and the same boundary conditions as for the laboratory experiments. The duration of the bacterial input suspension was 24 min to be consistent with the laboratory experiments. The model parameters for each column unit were given in Tables 1 and 2. The saturated hydraulic conductivity of the macropore domain was set equal to that of the fine sand matrix in the homogeneous column (Type 0), so there is no preferential flow path in this unit. The mean solute concentration at the bottom boundary for an entire virtual field is given by the ensemble average of the local concentrations in all stream tubes as described by the following equation:

$$C^*(t) = \frac{\langle q_i C_i(t)\rangle}{\langle q_i\rangle} = \frac{\sum_{i=1}^{n} f_i q_i C_i(t)}{\sum_{i=1}^{n} f_i q_i} \tag{6}$$

where $C^*(t)$ is the combined flux averaged effluent concentration of the virtual field at time t; f_i is the fraction of unit i; q_i is the flow rate of unit i; and $C_i(t)$ is the effluent concentration of unit i at time t. Another advantage of the stream tube model is that the variance in $C^*(t)$ may also be calculated as (Toride et al., 1995):

$$\sigma^2 = \frac{\sum_{i=1}^{n} f_i (q_i C_i(t) - \langle q_i C_i(t)\rangle)^2}{\langle q_i\rangle^2} \tag{7}$$

where σ is the standard deviation.

After obtaining the BTC of a virtual field with Eq. (6), we estimated a new set of dual-permeability model parameters for the virtual field. Only K_f^* and k_{fm}^* were fitted to the field BTC as all other parameters were the same for all units (Table 3). Figs. 5 and 6 show the ensemble and simulated BTCs of the virtual fields listed in Table 3 at IS equal to 1 and 20 mM, and standard deviation for each BTC. At IS = 1 mM, the ensemble BTCs were very similar to the typical BTC from laboratory experiments as shown in Fig. 3, and differences between the virtual fields were very small. Similar to what has been observed in transport experiments conducted at IS = 20 mM in Fig. 4, early breakthrough from the preferential path was observed while no significant breakthrough came from the matrix. The amount of breakthrough from the preferential path was positively correlated with the fractions of units with long lenses (Type I, Type II 19 cm, and Type IV 19 cm) as these units could transport more cells than the others.

Table 3
Examples of virtual fields with their fractions (f_i) for each unit, estimated model parameters, and R^2.

		IS = 20 mM				IS = 1 mM			
		Field 1	Field 2	Field 3	Field 4	Field 5	Field 6	Field 7	Field 8
f_i	Type 0	.24	.22	.18	.08	.32	.17	.17	.21
	Type I	.20	.05	.07	.16	.13	.25	.21	.21
	Type II 19 cm	.15	.07	.13	.15	.12	.02	.05	.07
	Type II 18 cm	.22	.14	.17	.19	.26	.22	.07	.22
	Type II 16 cm	.07	.18	.18	.22	.06	.05	.08	.03
	Type IV 19 cm	.08	.11	.12	.07	.02	.01	.22	.02
	Type IV 18 cm	.04	.23	.15	.13	.09	.28	.20	.24
K_f^* (cm/min)		8.7 ± 0.3	7.0 ± 0.5	7.5 ± 0.5	7.9 ± 0.6	5.8 ± 0.2	7.1 ± 0.1	7.1 ± 0.1	7.4 ± 0.6
k_{fm}^* (min^{-1})		$(7.8 \pm 0.8) * 10^{-4}$	$(10.4 \pm 1.6) * 10^{-4}$	$(9.5 \pm 1.2) * 10^{-4}$	$(9.0 \pm 1.5) * 10^{-4}$	$(1.6 \pm 0.1) * 10^{-4}$	$(2.4 \pm 0.2) * 10^{-4}$	$(2.9 \pm 0.2) * 10^{-4}$	$(2.6 \pm 0.9) * 10^{-4}$
R^2		.997	.989	.991	.990	.999	1.000	1.000	.999

It should be emphasized that virtual fields are a simplified representation of the natural environment. Nevertheless, the stream tube model has often been used to approximate flow and transport at the field scale (e.g., Dagan, 1984; Freyberg, 1986; Gelhar and Axness, 1983; Kabala and Sposito, 1991; Russo, 1991; Sposito and Barry, 1987) and available experimental data are generally consistent with this approach (Dean and Foran, 1992; Evans and Owens, 1972; Guzman et al., 2009). Furthermore, the estimated mean and variance in microbial concentrations are needed for risk assessment. Consequently, the outlined approach provides a relatively simple means to account for observed preferential flow and transport processes in virtual fields. Application of our dual-permeability stream tube approach to real field data would certainly be a worthwhile objective, but beyond the scope of the current manuscript.

5.2. Parameter upscaling

The field-scale values of K_f^* and k_{fm}^* were obtained in the previous section by fitting the dual-permeability model to the combined effluent concentrations. In this section we investigate ways to predict these parameters from properties of individual stream tubes. As the properties of the matrix were identical for all column units, they were the same for the virtual field as well. Simple averaging of hydraulic parameters has been used as one way of upscaling (Fleckenstein and Fogg, 2008; Renard and De

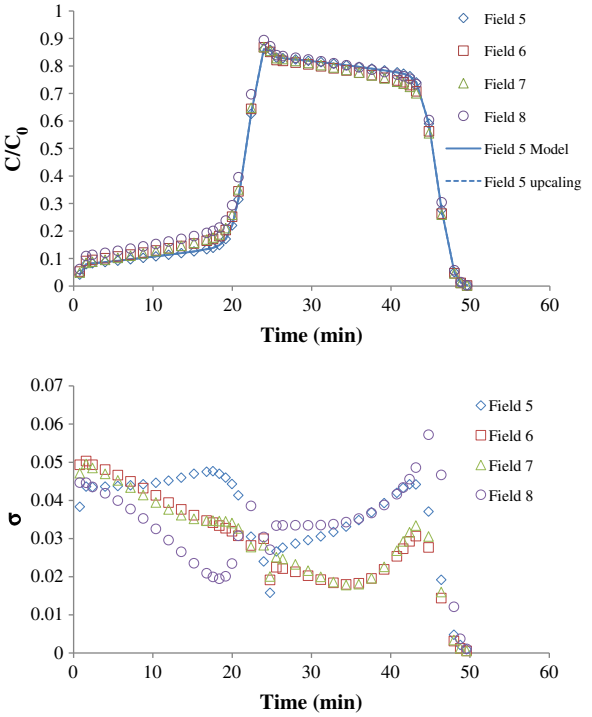

Fig. 5. BTCs of *E. coli* D21g at 1 mM from virtual fields (calculated using Eq. (6)), and simulations with inversely estimated (model) and upscaled (upscaling; using Eqs. (9) and (11)) model parameters, and standard deviation σ of BTCs from virtual fields as a function of time. Not all simulations are plotted as they mimic virtual field data.

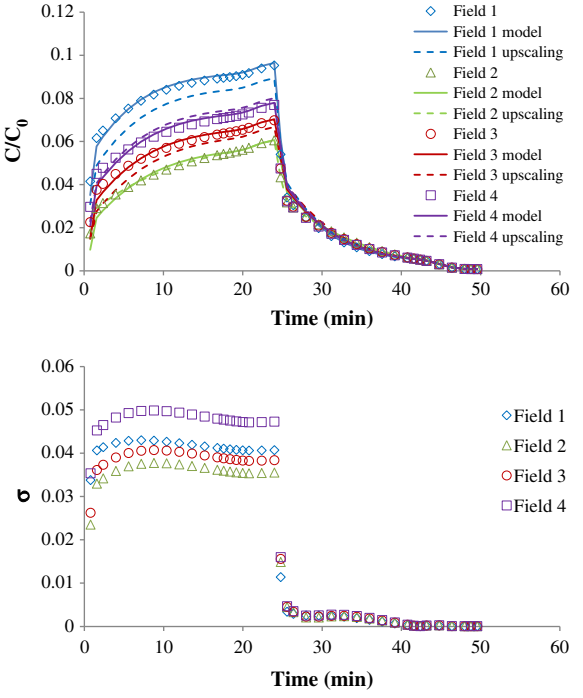

Fig. 6. BTCs of *E. coli* D21g at 20 mM from virtual fields (calculated using Eq. (6)) and simulations with inversely estimated (model) and upscaled (upscaling; using Eqs. (9) and (11)) model parameters, and standard deviation σ of BTCs from virtual fields as a function of time.

Marsily, 1997; Wen and Gómez-Hernández, 1996). Different techniques for averaging relevant parameters can be applied, such as arithmetic, geometrical, and harmonic means. Several methods were investigated to predict the upscaled parameters K_f^* and k_{fm}^* for the virtual fields as follows:

$$K_{f*} = \frac{\sum_{i=1}^{n} f_i K_{f,i}}{\sum_{i=1}^{n} f_i} \tag{8}$$

$$K_{f*} = \frac{\sum_{i=1}^{n} f_i K^2_{f,i}}{\sum_{i=1}^{n} f_i K_{f,i}} \tag{9}$$

$$k_{fm*} = \frac{\sum_{i=1}^{n} f_i k_{fm,i}}{\sum_{i=1}^{n} f_i} \tag{10}$$

$$k_{fm*} = \frac{\sum_{i=1}^{n} f_i}{\sum_{i=1}^{n} \frac{f_i}{k_{fm,i}}}. \tag{11}$$

Eqs. (8) and (10) assume that an upscaled parameter can be determined as a simple linear combination of local parameters. Conversely, Eqs. (9) and (11) assume a nonlinear relationship between field and column-scale parameters. Since the flux through the macropore and the preferential transport of microbes are both correlated with K_f, Eq. (9) relates K_f^* to a flux weighted average of K_f. Eq. (11) considers that k_{fm}^* is related to the harmonic mean of k_{fm}. This relationship seems plausible because larger values of k_{fm} produce greater mass transfer at the matrix–macropore interface, and thus higher microbe retention in the matrix and less transport of microbes through the macropore.

Table 4 lists the upscaled model parameters obtained from Eqs. (8)–(11) for the virtual fields listed in Table 3. The simulated BTCs with Eq. (9) for K_f^* and Eq. (11) for k_{fm}^* matched the BTCs of the virtual fields the best ($R^2 > 0.98$) (Figs. 5 and 6). Similar upscaling procedures were tested for virtual fields generated with different hydraulic conductivities for the matrix and macropore, and for various fractions of the total soil occupied by the macropore system. Eqs. (9) and (11) again provided a good description of the field-scale BTCs. Consequently, the upscaled model parameters given by Eqs. (9) and (11) provided a reasonable prediction of the transport of microorganism in the considered virtual fields.

6. Conclusions

Dual-permeability models were able to describe the transport of bromide and *E. coli* D21g at both high and low IS conditions when optimized parameters were used. However, forward simulation of *E. coli* D21g based on information from transport experiments with *E. coli* D21g in homogeneous columns and from transport experiments with bromide in columns with preferential flow could not describe some features of transport of *E. coli* D21g at both high and low IS.

Inverse estimation indicated strong correlations between the parameters of the dual-permeability model (e.g., hydraulic conductivity of the macropore, mass transfer coefficient) and the configuration and length of the preferential path. In general, 1) the hydraulic conductivity of the macropore decreased with a decrease in lens length; 2) the mass transfer coefficient increased with a decrease in lens length, and Type IV lens configuration produced greater mass transfer rate; and 3) *E. coli* D21g had a similar mass transfer coefficient as bromide at low IS, but the mass transfer coefficient was much

Table 4
Upscaled model parameters obtained by different methods.

		Field 1	Field 2	Field 3	Field 4
K_f^* (cm/min)	Eq. (7)	6.5	5.9	6.3	7.3
	Eq. (8)	8.8	7.7	7.9	8.3
k_{fm}^* (min^{-1})	Eq. (9)	$7.8 * 10^{-4}$	$14.0 * 10^{-4}$	$12.5 * 10^{-4}$	$13.3 * 10^{-4}$
	Eq. (10)	$9.3 * 10^{-4}$	$14.6 * 10^{-4}$	$11.7 * 10^{-4}$	$9.6 * 10^{-4}$

greater for *E. coli* D21g at high IS compared to a low IS and that of bromide.

The fitted dual-permeability model parameters that were obtained at the column-scale were subsequently used to predict the BTCs of virtual fields are composed of preferential flow paths of various lengths and configurations using a linear superposition approach. The field-scale BTCs were successfully described using the dual-permeability model. Methods to predict the upscaled dual-permeability model parameters from local column parameters were then investigated. Eqs. (9) and (11) provided an accurate prediction of the transport of *E. coli* D21g in the virtual fields. However, the studied cases were still very limited compared to the possible situations in the field. For instance, the dual-permeability model predicts only two peaks (one from preferential flow and one from matrix flow). If the duration of the microorganism application is very short and the arrival times from different local preferential flow pathways vary a lot, the ensemble BTCs for the field could show multiple peaks. In this case, stochastic models may perform better than the dual-permeability model. Despite these acknowledged limitations, the dual-permeability model and upscaling approach presented herein appear to be viable first approximation to determine the effects of preferential flow on microbial transport at the field-scale under saturated conditions.

Acknowledgments

This research was supported in part by the USDA, ARS, NP 214, and Multistate Research Funded project W-2188. The USDA is an equal opportunity provider and employer.

References

Abbaszadegan, M., LeChevallier, M.W., Gerba, C.P., 2003. Occurrence of viruses in US groundwaters. J. Am. Water Works Assoc. 95, 107–120.

Abu-Ashour, J., Joy, D.M., Lee, H., Whiteley, H.R., Zelin, S., 1994. Transport of microorganisms through soil. Water Air Soil Pollut. 75 (1–2), 141–158.

Adamczyk, Z., Siwek, B., Zembala, M., Belouschek, P., 1994. Kinetics of localized adsorption of colloid particles. Adv. Colloid Interf. Sci. 48, 151–280.

Allaire, S.E., Gupta, S.C., Nieber, J., Moncrief, J.F., 2002. Role of macropore continuity and tortuosity on solute transport in soils: 1. Effects of initial and boundary conditions. J. Contam. Hydrol. 58 (3–4), 299–321.

Allaire-Leung, S.E., Gupta, S.C., Moncrief, J.F., 2000. Water and solute movement in soil as influenced by macropore characteristics—1. Macropore continuity. J. Contam. Hydrol. 41 (3–4), 283–301.

Anderson, S., Wang, H., Peyton, R., Gantzer, C., 2003. Estimation of porosity and hydraulic conductivity from X-ray CT-measured solute breakthrough. Geol. Soc. Lond., Spec. Publ. 215 (1), 135–149.

Andreu, L., Moreno, F., Jarvis, N., Vachaud, G., 1994. Application of the model MACRO to water movement and salt leaching in drained and irrigated marsh soils, Marismas, Spain. Agric. Water Manag. 25 (1), 71–88.

Arora, B., Mohanty, B.P., McGuire, J.T., 2011. Inverse estimation of parameters for multidomain flow models in soil columns with different macropore densities. Water Resour. Res. 47 (4), W04512.

Arora, B., Mohanty, B.P., McGuire, J.T., 2012. Uncertainty in dual permeability model parameters for structured soils. Water Resour. Res. 48 (1), W01524.

Bales, R.C., Gerba, C.P., Grondin, G.H., Jensen, S.L., 1989. Bacteriophage transport in sandy soil and fractured tuff. Appl. Environ. Microbiol. 55 (8), 2061–2067.

Beven, K., Germann, P., 1982. Macropores and water flow in soils. Water Resour. Res. 18 (5), 1311–1325.

Borchardt, M.A., Bertz, P.D., Spencer, S.K., Battigelli, D.A., 2003. Incidence of enteric viruses in groundwater from household wells in Wisconsin. Appl. Environ. Microbiol. 69, 1172–1180.

Bradford, S.A., Kim, H., 2010. Implications of cation exchange on clay release and colloid-facilitated transport in porous media. J. Environ. Qual. 39 (6), 2040–2046.

Bradford, S.A., Bettahar, M., Simunek, J., van Genuchten, M.T., 2004. Straining and attachment of colloids in physically heterogeneous porous media. Vadose Zone J. 3 (2), 384–394.

Bradford, S.A., Šimůnek, J., Bettahar, M., van Genuchten, M.T., Yates, S.R., 2006. Significance of straining in colloid deposition: evidence and implications. Water Resour. Res. 42 (12).

Castiglione, P., Mohanty, B.P., Shouse, P.J., Šimůnek, J., van Genuchten, M.T., Santini, A., 2003. Lateral water diffusion in an artificial macroporous system: modeling and experimental evidence. Vadose Zone J. 2 (2), 212–221.

Cey, E.E., Rudolph, D.L., Passmore, J., 2009. Influence of macroporosity on preferential solute and colloid transport in unsaturated field soils. J. Contam. Hydrol. 107 (1–2), 45–57.

Chen, G.X., Walker, S.L., 2007. Role of solution chemistry and ion valence on the adhesion kinetics of groundwater and marine bacteria. Langmuir 23 (13), 7162–7169.

Dagan, G., 1984. Solute transport in heterogeneous porous formations. J. Fluid Mech. 145, 151–177.

Dagan, G., 1993. Higher-order correction of effective conductivity of heterogeneous formations of lognormal conductivity distribution. Transp Porous Media 12, 279–290.

Dean, D.M., Foran, M.E., 1992. The effect of farm liquid waste application on tile drainage. J. Soil Water Conserv. 47 (5), 368–369.

Dong, H., Onstott, T.C., DeFlaun, M.F., Fuller, M.E., Scheibe, T.D., Streger, S.H., Rothmel, R.K., Mailloux, B.J., 2002. Relative dominance of physical versus chemical effects on the transport of adhesion-deficient bacteria in intact cores from South Oyster, Virginia. Environ. Sci. Technol. 36 (5), 891–900.

Evans, M.R., Owens, J.D., 1972. Factors affecting the concentration of faecal bacteria in land-drainage water. J. Gen. Microbiol. 71 (3), 477–485.

Fleckenstein, J.H., Fogg, G.E., 2008. Efficient upscaling of hydraulic conductivity in heterogeneous alluvial aquifers. Hydrogeol. J. 16 (7), 1239–1250.

Flury, M., Flühler, H., Jury, W.A., Leuenberger, J., 1994. Susceptibility of soils to preferential flow of water: a field study. Water Resour. Res. 30 (7), 1945–1954.

Fontes, D.E., Mills, A.L., Hornberger, G.M., Herman, J.S., 1991. Physical and chemical factors influencing transport of microorganisms through porous media. Appl. Environ. Microbiol. 57 (9), 2473–2481.

Freyberg, D.L., 1986. A natural gradient experiment on solute transport in a sand aquifer: 2. Spatial moments and the advection and dispersion of nonreactive tracers. Water Resour. Res. 22 (13), 2031–2046.

Gelhar, L.W., Axness, C.L., 1983. Three-dimensional stochastic analysis of macrodispersion in aquifers. Water Resour. Res. 19 (1), 161–180.

Greco, R., 2002. Preferential flow in macroporous swelling soil with internal catchment: model development and applications. J. Hydrol. 269 (3), 150–168.

Guzman, J.A., Fox, G.A., Malone, R.W., Kanwar, R.S., 2009. Transport from surface-applied manure to subsurface drains through artificial biopores. J. Environ. Qual. 38 (6), 2412–2421.

Gwo, J., Jardine, P., Wilson, G., Yeh, G., 1995. A multiple-pore-region concept to modeling mass transfer in subsurface media. J. Hydrol. 164 (1), 217–237.

Gwo, J., Jardine, P., Wilson, G., Yeh, G., 1996. Using a multiregion model to study the effects of advective and diffusive mass transfer on local physical nonequilibrium and solute mobility in a structured soil. Water Resour. Res. 32 (3), 561–570.

Hendry, M.J., Lawrence, J.R., Maloszewski, P., 1999. Effects of velocity on the transport of two bacteria through saturated sand. Ground Water 37 (1), 103–112.

Jarvis, N., Jansson, P.E., Dik, P., Messing, I., 1991. Modelling water and solute transport in macroporous soil. I. Model description and sensitivity analysis. J. Soil Sci. 42 (1), 59–70.

Jiang, S., Pang, L.P., Buchan, G.D., Šimůnek, J., Noonan, M.J., Close, M.E., 2010. Modeling water flow and bacterial transport in undisturbed lysimeters under irrigations of dairy shed effluent and water using HYDRUS-1D. Water Res. 44 (4), 1050–1061.

Jury, W.A., Roth, K., 1990. Transfer Functions and Solute Movement Through Soil: Theory and Applications. Birkhäuser Verlag AG.

Kabala, Z., Sposito, G., 1991. A stochastic model of reactive solute transport with time-varying velocity in a heterogeneous aquifer. Water Resour. Res. 27 (3), 341–350.

Kohler, A., Abbaspour, K., Fritsch, M., van Genuchten, M.T., Schulin, R., 2001. Simulating unsaturated flow and transport in a macroporous soil to tile drains subject to an entrance head: model development and preliminary evaluation. J. Hydrol. 254 (1), 67–81.

Köhne, J.M., Köhne, S., Šimůnek, J., 2009a. A review of model applications for structured soils: a) water flow and tracer transport. J. Contam. Hydrol. 104 (1–4), 4–35.

Köhne, J.M., Köhne, S., Šimůnek, J., 2009b. A review of model applications for structured soils: b) pesticide transport. J. Contam. Hydrol. 104 (1–4), 36–60.
Kung, K.-J.S., Hanke, M., Helling, C.S., Kladivko, E.J., Gish, T.J., Steenhuis, T.S., Jaynes, D.B., 2005. Quantifying pore-size spectrum of macropore-type preferential pathways. Soil Sci. Soc. Am. J. 69 (4), 1196–1208.
Larsson, M., Jarvis, N., 1999a. Evaluation of a dual-porosity model to predict field-scale solute transport in a macroporous soil. J. Hydrol. 215 (1), 153–171.
Larsson, M.H., Jarvis, N.J., 1999b. A dual-porosity model to quantify macropore flow effects on nitrate leaching. J. Environ. Qual. 28 (4), 1298–1307.
Leij, F.J., Bradford, S.A., 2009. Combined physical and chemical nonequilibrium transport model: analytical solution, moments, and application to colloids. J. Contam. Hydrol. 110 (3–4), 87–99.
Madsen, E.L., Alexander, M., 1982. Transport of Rhizobium and Pseudomonas through soil1. Soil Sci. Soc. Am. J. 46 (3), 557–560.
Mccaulou, D.R., Bales, R.C., Arnold, R.G., 1995. Effect of temperature-controlled motility on transport of bacteria and microspheres through saturated sediment. Water Resour. Res. 31 (2), 271–280.
Mills, A.L., Herman, J.S., Hornberger, G.M., Dejesus, T.H., 1994. Effect of solution ionic-strength and iron coatings on mineral grains on the sorption of bacterial-cells to quartz sand. Appl. Environ. Microbiol. 60 (9), 3300–3306.
Monga, O., Ndeye Ngom, F., François Delerue, J., 2007. Representing geometric structures in 3D tomography soil images: application to pore-space modeling. Comput. Geosci. 33 (9), 1140–1161.
Morley, L.M., Hornberger, G.M., Mills, A.L., Herman, J.S., 1998. Effects of transverse mixing on transport of bacteria through heterogeneous porous media. Water Resour. Res. 34 (8), 1901–1908.
Pivetz, B., Steenhuis, T., 1995. Soil matrix and macropore biodegradation of 2, 4-D. J. Environ. Qual. 24 (4), 564–570.
Renard, P., De Marsily, G., 1997. Calculating equivalent permeability: a review. Adv. Water Resour. 20 (5), 253–278.
Russo, D., 1991. Stochastic analysis of simulated vadose zone solute transport in a vertical cross section of heterogeneous soil during nonsteady water flow. Water Resour. Res. 27 (3), 267–283.
Saiers, J.E., Hornberger, G.M., Harvey, C., 1994. Colloidal silica transport through structured, heterogeneous porous media. J. Hydrol. 163 (3), 271–288.
Schelle, H., Durner, W., Schlüter, S., Vogel, H.-J., Vanderborght, J., 2013. Virtual soils: moisture measurements and their interpretation by inverse modeling. Vadose Zone J. 12 (3). http://dx.doi.org/10.2136/vzj2012.0168 (12 pp.).
Schijven, J.K., Hassanizadeh, S.M., 2000. Removal of viruses by soil passage: overview of modeling, processes, and parameters. Crit. Rev. Environ. Sci. Technol. 30, 49–127.
Šimůnek, J., Jarvis, N.J., van Genuchten, M.T., Gärdenäs, A., 2003. Review and comparison of models for describing non-equilibrium and preferential flow and transport in the vadose zone. J. Hydrol. 272 (1–4), 14–35.
Šimůnek, J., van Genuchten, M.T., Šejna, M., 2008. Development and applications of the HYDRUS and STANMOD software packages and related codes. Vadose Zone J. 7, 587–600.
Singh, P., Kanwar, R.S., 1991. Preferential solute transport through macropores in large undisturbed saturated soil columns. J. Environ. Qual. 20 (1), 295–300.
Sposito, G., Barry, D., 1987. On the Dagan model of solute transport in groundwater: foundational aspects. Water Resour. Res. 23 (10), 1867–1875.
Toride, N., Leij, F.J., van Genuchten, M.Th, 1995. The CXTFIT Code for Estimating Transport Parameters from Laboratory or Filed Tracer Experiments. US Salinity Laboratory, Riverside.
U.S. Environmental Protection Agency, 1997. National Water Quality Inventory, Report to Congress. Rep.841-R-97-008. USEPA, Washington, DC.
Unc, A., Goss, M.J., 2003. Movement of faecal bacteria through the vadose zone. Water Air Soil Pollut. 149 (1–4), 327–337.
Wang, Y., Bradford, S.A., Šimůnek, J., 2013. Transport and fate of microorganisms in soils with preferential flow under different solution chemistry conditions. Water Resour. Res. 49 (5), 2424–2436.
Wang, Y., Bradford, S.A., Šimůnek, J., 2014. Physicochemical factors influencing the preferential transport of *Escherichia coli* in soils. Vadose Zone J. 13 (1). http://dx.doi.org/10.2136/vzj2013.07.0120 (10 pp.).
Wen, X.-H., Gómez-Hernández, J.J., 1996. Upscaling hydraulic conductivities in heterogeneous media: an overview. J. Hydrol. 183 (1), ix–xxxii.
Wollum, A., Cassel, D., 1978. Transport of microorganisms in sand columns. Soil Sci. Soc. Am. J. 42 (1), 72–76.
Yee, N., Fein, J.B., Daughney, C.J., 2000. Experimental study of the pH, ionic strength, and reversibility behavior of bacteria–mineral adsorption. Geochim. Cosmochim. Acta 64 (4), 609–617.